Science Advances
AAAS

Supplementary Materials for

Imaging and simulation of surface plasmon polaritons on layered 2D MXenes

Janek Rieger *et al.*

Corresponding author: Sarah B. King, sbking@uchicago.edu

Sci. Adv. **11**, eads3689 (2025)
DOI: 10.1126/sciadv.ads3689

This PDF file includes:

Supplementary Text

Details of investigated MXene flakes

All investigated flakes were characterized by optical microscopy and atomic force microscopy (AFM). The optical images show a larger field of view around the investigated flakes. They also show that investigated flakes are mostly transparent in the visible region. AFM was used to determine the thickness of the investigated MXene flakes. Figure S1 shows the images and linecuts of the two flakes (Flake 1 and Flake 2) that are characterized in detail with nP-PEEM and discussed in the main text. Flake 1 exhibits fringes in nP-PEEM. Its thickness is approximately d=160 nm (see Fig. S1C). In contrast, Flake 2 is only approximately d=25 nm thick. This flake doesn't show fringes in nP-PEEM experiments.

Figures S2 and S3 show corresponding optical and AFM images from two additional flakes (Flake 3 and Flake 4). Both flakes show fringes on their surface in nP-PEEM measurements. Their dispersion was plotted in Figure 3 of the main text. A comparison of 1P-PEEM and nP-PEEM images from the two flakes is shown in Figure S2D-F and in Figure S3D-F, respectively. The behavior of both flakes in PEEM is comparable to the behavior of Flake 1. No fringes are observed in the 1P-PEEM images (see Figs. S2D and S3D). Fringes can be observed in nP-PEEM when the laser polarization is perpendicular to flake edges (see Figs. S2E, F and S3E, F). Note that both flakes are thicker than the critical thickness of approximately 30 nm that is necessary to observe the fringes (see discussion in main text for details).

Dielectric function of $Ti_3C_2T_x$ and plasmon modes of metallic thin films

The dielectric function, $\epsilon(\omega) = \epsilon'(\omega) + i\epsilon''(\omega)$, of $Ti_3C_2T_x$ from reference (23) is presented in Figure S4A. Interband transitions cause peaks in the imaginary part ϵ''. Surface plasmons can exist for regions where the real part ϵ' is negative. This is mostly the case for energies <1.9 eV as can be seen from Figure S4A.

The surface plasmons with wavevector k_x from the two interfaces of a metallic thin film with thickness d interact when $k_x * d \ll 1$ (53). Figure S4B shows the dispersion of the two hybridized surface plasmon modes of a d=100 nm thick metallic film on SiO_2 in vacuum. The metallic film is modeled with the Drude model (with a bulk plasmon energy $\omega_P = 5.9$ eV a damping of $\Gamma = 0.2$ eV, and $\epsilon_\infty = 1$). These values are based on the conductivity values of $Ti_3C_2T_x$ from Shamsabadi et al. (23). In this model, the interband transitions of $Ti_3C_2T_x$ were neglected for clarity. The two hybridized modes in Figure S4B show different intensities since the thin film is embedded between vacuum and SiO_2. This asymmetric cladding also changes the confinement of the two modes. The asymmetric mode (red marker in Fig. S4B is located at the interface to the SiO_2 (see Fig. S4C and E). The symmetric mode (green marker in Fig. S4B) is located at the interface to vacuum (see Fig. S4D and F).

Overview over all linecuts and fits

Photon energy-dependent nP-PEEM measurements were carried out on all three presented flakes. Linecuts with a width of 25 pixels ($\sim 350 - 400$ nm) were taken from the nP-PEEM images to determine the dispersion of the fringes. The non-oscillatory background of the linecuts was determined individually by building the median over approximately 50-100 pixels for each linecut.

The median was subtracted from the linecuts to remove of the background. The background-corrected linecuts were fitted with the function $f(x) = A_0 e^{(-l*x)} * \sin(k_x x - \phi) + bx + c$ to determine the corresponding wavevectors k_x. A_0 is the initial amplitude, l the decay constant, ϕ the phase of the fringes with respect to the coordinate x, and k_x is the wavevector. Figure S5 shows all examined linecuts and corresponding fits.

Surface electronic structure and power-dependence of nP-PEEM

The utilized photoelectron microscope from Focus GmbH has a high-pass energy filter in its imaging column. It can be used to filter for photoelectrons with a kinetic energy higher than the pass energy. That way, photoelectron energy-dependent PEEM images can be measured. Photoelectron spectra with a resolution of approximately 50 meV are generated by calculating the first derivative of the energy-dependent photoemission intensities. Figure S6A shows an energy-integrated 1P-PEEM image of Flake 1 and Flake 2. Additional flakes can be identified due to a larger field of view. Photoelectron spectra were generated for three regions of interest (ROI) on three different flakes, which are indicated in the PEEM image in Figure S6A. They are shown in Figure S6B. All three spectra look similar. Hence, all three flakes have a similar electronic surface structure. Their work function is approximately 4.8 eV as determined with an error function from the lower-kinetic edge of the photoelectron spectra. Based on that work function, nP-PEEM experiments on Flakes 1 and 2 with photon energies $h\nu < 4.8$ eV correspond to 2P-PEEM, $h\nu < 2.4$ eV to 3P-PEEM, and $h\nu < 1.6$ eV to 4P-PEEM. The latter was confirmed by performing laser pulse power-dependent nP-PEEM with $h\nu = 1.51$ eV on the flake that shows fringes (see Fig. S6C). The power-dependent intensity shows approximately a x^4 dependence as expected for 4P-PEEM (see Fig. S6D). Such a highly nonlinear excitation indicates enhanced local fields at the surface.

nP-PEEM experiments with grazing incidence

The electric field of the laser pulse needs to be considered for the interpretation of fringes in nP-PEEM experiments. nP-PEEM probes the coherent superposition of electric fields excited at the surface with the fields of the laser pulse. Hence, the measured fringe pattern depends on the angle of incidence of the laser pulse (43, 61). Figure S7 shows a comparison between nP-PEEM images for near-normal ($\theta \approx 4°$) and grazing incidence ($\theta \approx 65°$), respectively. The plane of grazing incidence is horizontally aligned to the shown PEEM images, and the laser is incident from the left side. Experimental nP-PEEM images were recorded on Flake 4 (compare Fig. S7B and E). Simulated nP-PEEM images from FDTD are shown in Figure S7C and F. Experimental and simulated nP-PEEM images are in very good agreement. The observed fringes under grazing incidence exhibit a behavior that is characteristic of surface plasmon polaritons (SPP). SPPs can be launched from the left and right edge of Flake 4. Their fringe spacing should resemble an interference pattern with the following wavelength λ_F (39):

$$\lambda_F = \frac{\lambda_L * \lambda_{SPP}}{\sqrt{\lambda_L^2 + \lambda_{SPP}^2 - 2 * \lambda_L * \lambda_{SPP} * \cos(\gamma)}}$$

Where γ denotes the in-plane angle of between the propagation vectors k_L and k_{SPP}, λ_{SPP} the wavelength of the SPP, and $\lambda_L = \frac{\lambda}{\sin(\theta)}$ the wavelength of the laser pulse projected onto the surface. The orientation of the two considered edges of Flake 4 with respect to the light propagation vector k_L is $16°$ and $180°$, respectively. SPPs that are launched from the left edge of Flake 4 should

exhibit a wavelength around 2.67 µm, while the SPPs that are launched from the right edge should exhibit a much shorter wavelength around 0.39 µm. The measured and simulated nP-PEEM images in Figure S7E and F show this behavior. A large fringe spacing on the order of several µm can be observed next to the left edge. The fringe spacing at the right edge is much smaller and on the order of several 100 nm.

Impact of anisotropy on nP-PEEM images

The experimental nP-PEEM data is reasonably well-described with simulations based on an isotropic dielectric function of $Ti_3C_2T_x$ (see Dispersion in Fig. 3 of the main text). However, it is more plausible that an anisotropic dielectric function is assumed for $Ti_3C_2T_x$ since it is a layered material (see Discussion in main text). Figure S8 compares simulated nP-PEEM images from a $Ti_3C_2T_x$ flake with an isotropic dielectric function with the ones from a $Ti_3C_2T_x$ flake with an anisotropic dielectric function. The dielectric function from Shamsabadi et al. (23) was used for the isotropic case. It was also used for the in-plane ($\epsilon_{x,y}$) part of the anisotropic dielectric function. The out-of-plane part of the anisotropic dielectric was set to a constant real value of $\epsilon_z = 3.8$ which corresponds to the ϵ_∞ of $\epsilon_{x,y}$. This resembles a highly anisotropic dielectric with no conduction or interband transitions in the out-of-plane direction. The comparison in Figure S8 shows that the SPPs in the nP-PEEM images at < 1.9 eV are slightly more pronounced when an anisotropic dielectric function is assumed (compare Fig. S8A and E). In contrast, the waveguides at > 1.9 eV have a slightly lower photoemission background (compare Fig. S8B and F). However, the wavevectors are barely impacted by the anisotropy. They are $k = 9.11 \pm 0.03$ µm^{-1} at 1.7 eV and $k = 13.94 \pm 0.01$ µm^{-1} at 2.7 eV, respectively, when an isotropic dielectric is assumed. An anisotropic dielectric yield $k = 9.16 \pm 0.03$ µm^{-1} at 1.7 eV and $k = 14.01 \pm 0.01$ µm^{-1} at 2.7 eV, respectively.

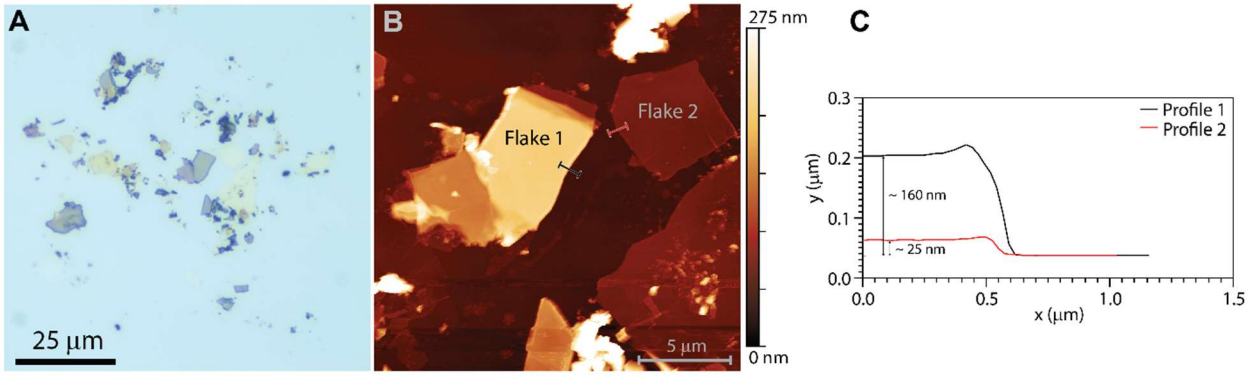

Fig. S1. Optical and AFM image of the two MXene flakes (Flake 1 and Flake 2) that are discussed in detail in the main text. (A) shows the optical image of the region around the flake. (B) presents the corresponding AFM image. (C) shows two linecuts taken from and indicated in the AFM image in (B).

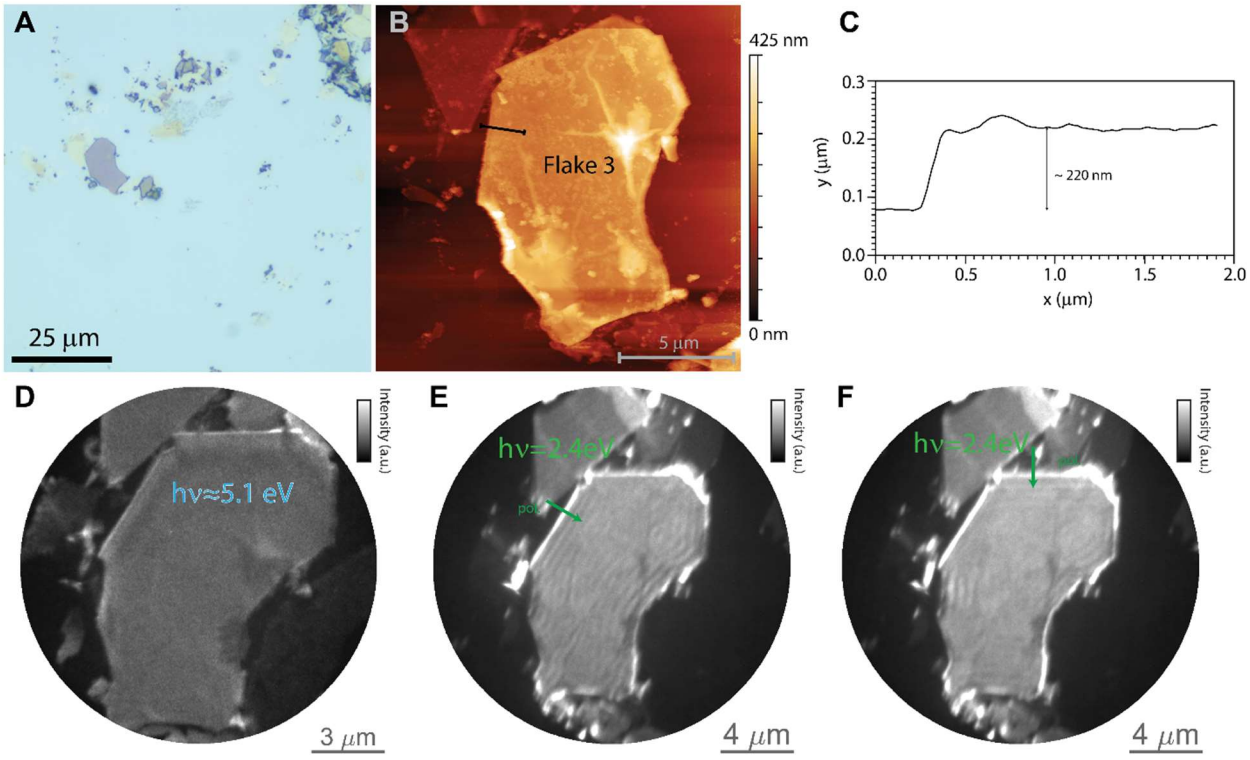

Fig. S2. Characterization of Flake 3. (A) Optical and (B) AFM images of the flake and surrounding region. (C) Linecut across the edge of the flake taken from and indicated in the AFM image in (B). (D) 1P-PEEM image from the flake. (E, F) 2P-PEEM images with laser polarization perpendicular to the indicated edges.

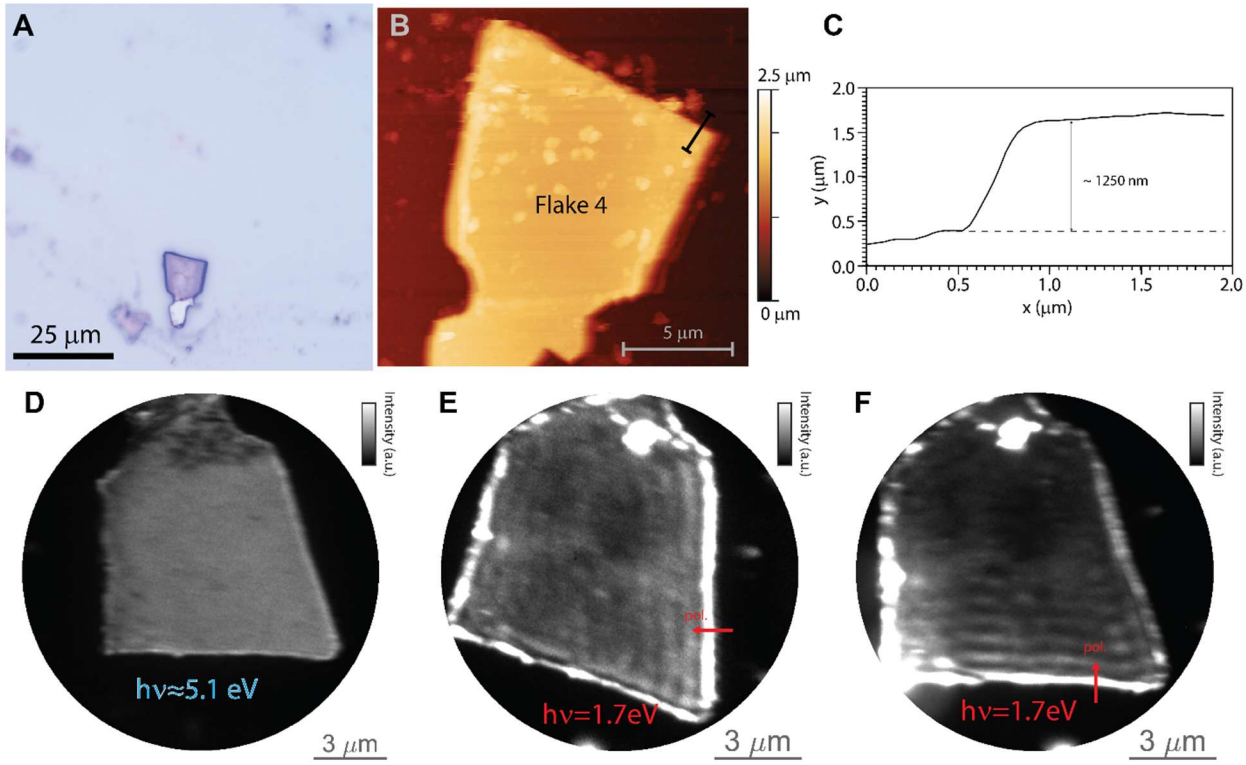

Fig. S3. Characterization of Flake 4. (A) Optical and (B) AFM images of the flake and surrounding region. (C) Linecut across the edge of the flake taken from and indicated in the AFM image in (B). (D) 1P-PEEM image from the flake. (E, F) 2P-PEEM images with laser polarization perpendicular to the indicated edges.

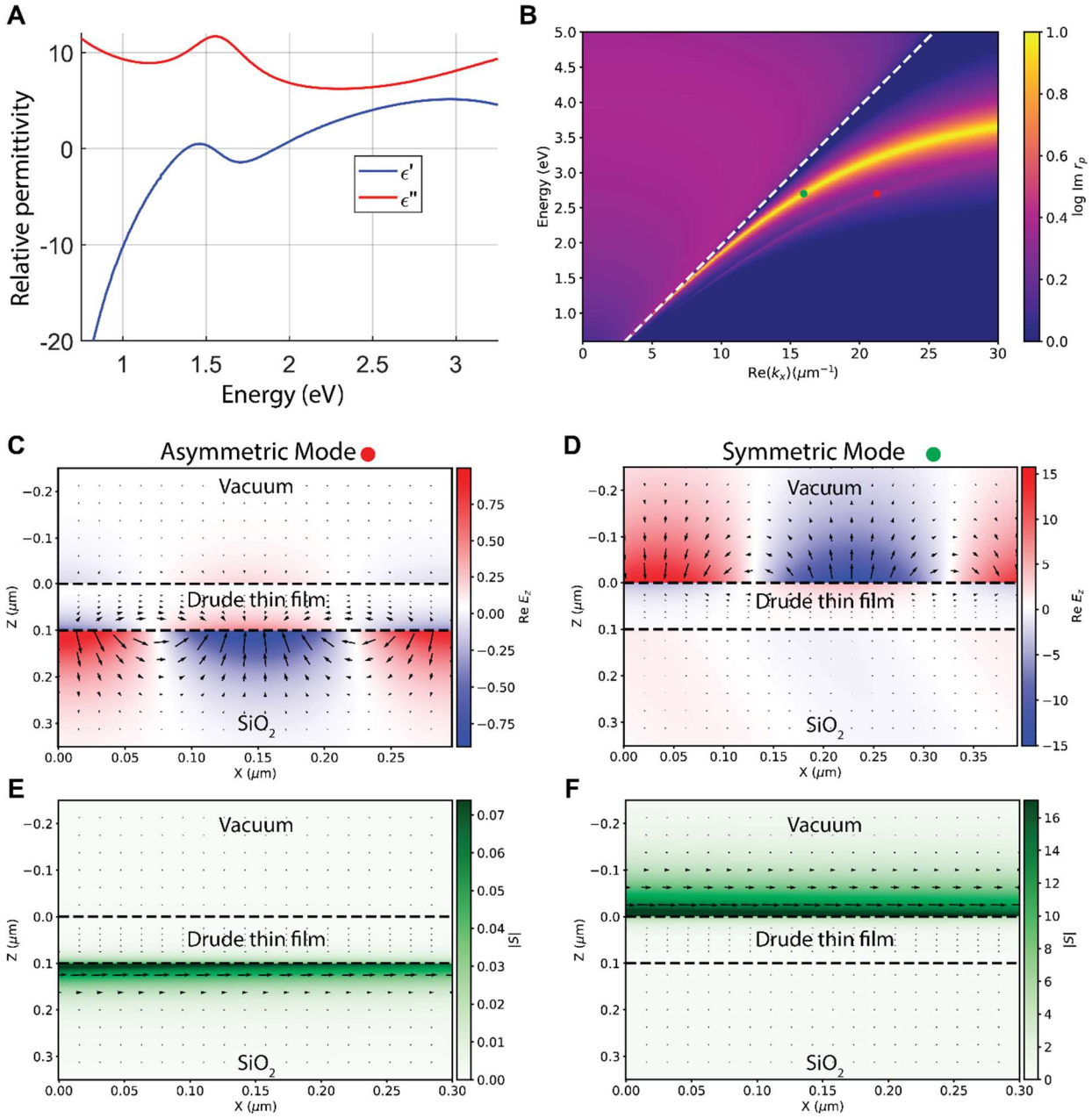

Fig. S4. Dielectric function of $Ti_3C_2T_x$ and plasmon modes of thin films. (A) Dielectric function of $Ti_3C_2T_x$ from Shamsabadi et al. (23). (B) Surface plasmon dispersion on a d=100 nm thick illustrative model Drude metal thin film between vacuum and SiO_2 with parameters, $\boldsymbol{\omega_P = 5.9\ eV, \gamma = 0.2\ eV, \epsilon_\infty = 1}$. This is only an illustrative model and not meant to illustrate the plasma frequencies of the MXenes studied in this work. (C) and (D) E_z fields across a model metallic thin film between vacuum and SiO_2 that are associated with the two surface plasmon modes from (B). (E) and (F) Poynting vectors across a model Drude metallic thin film between vacuum and SiO_2 that are associated with the two surface plasmon modes from (B). The energy and momentum of the modes whose fields and Poynting vectors are presented in (C) - (F) are indicated by a red and a green marker in (B).

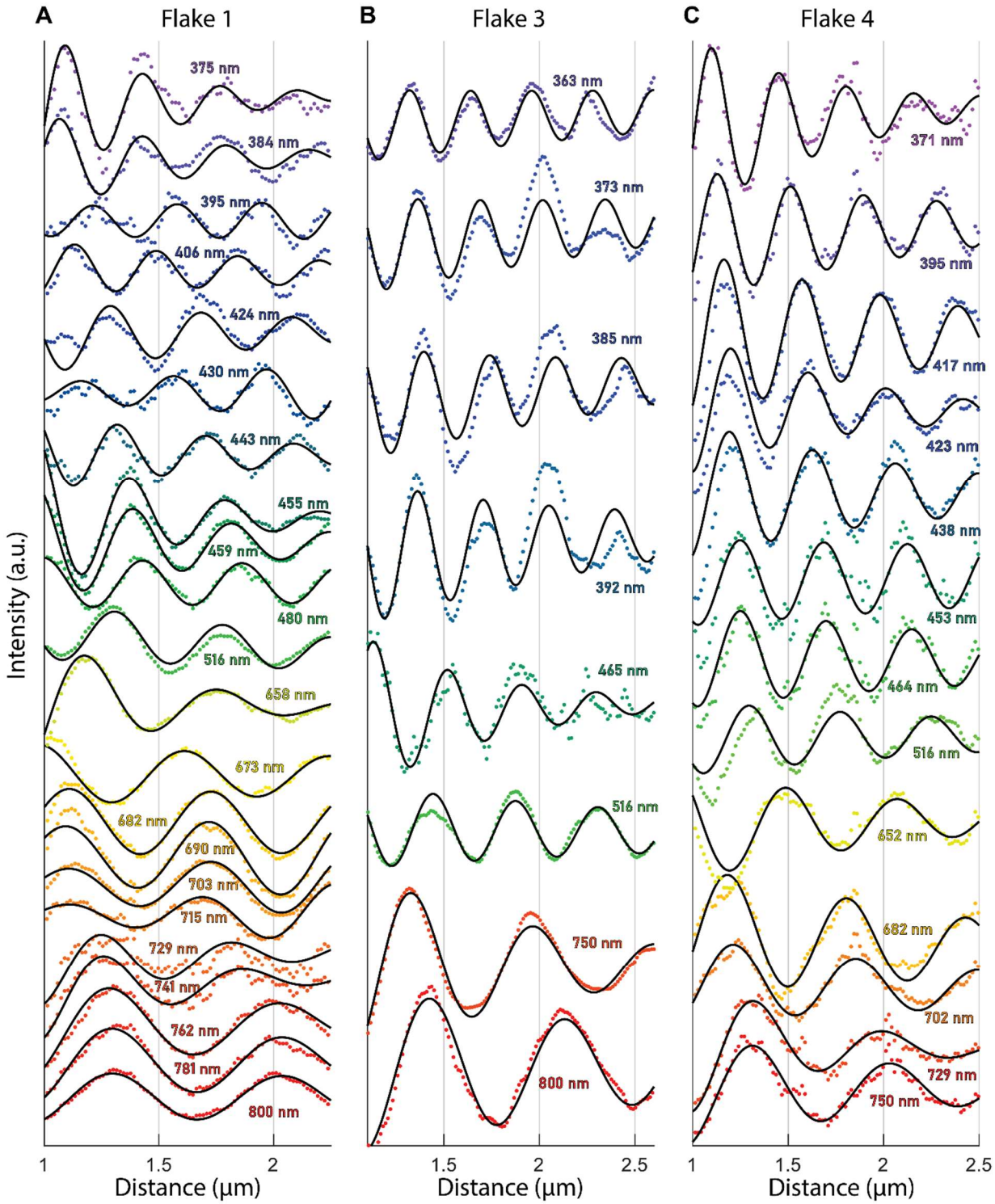

Fig. S5. Overview of all presented linecuts and corresponding fits from nP-PEEM measurements on flakes 1, 3, and 4. (A) Linecuts and fits from Flake 1 that was discussed in the main text. (B) Linecuts and fits from Flake 3. (C) Linecuts and fits from Flake 4. The linecuts are labeled with the corresponding excitation wavelength.

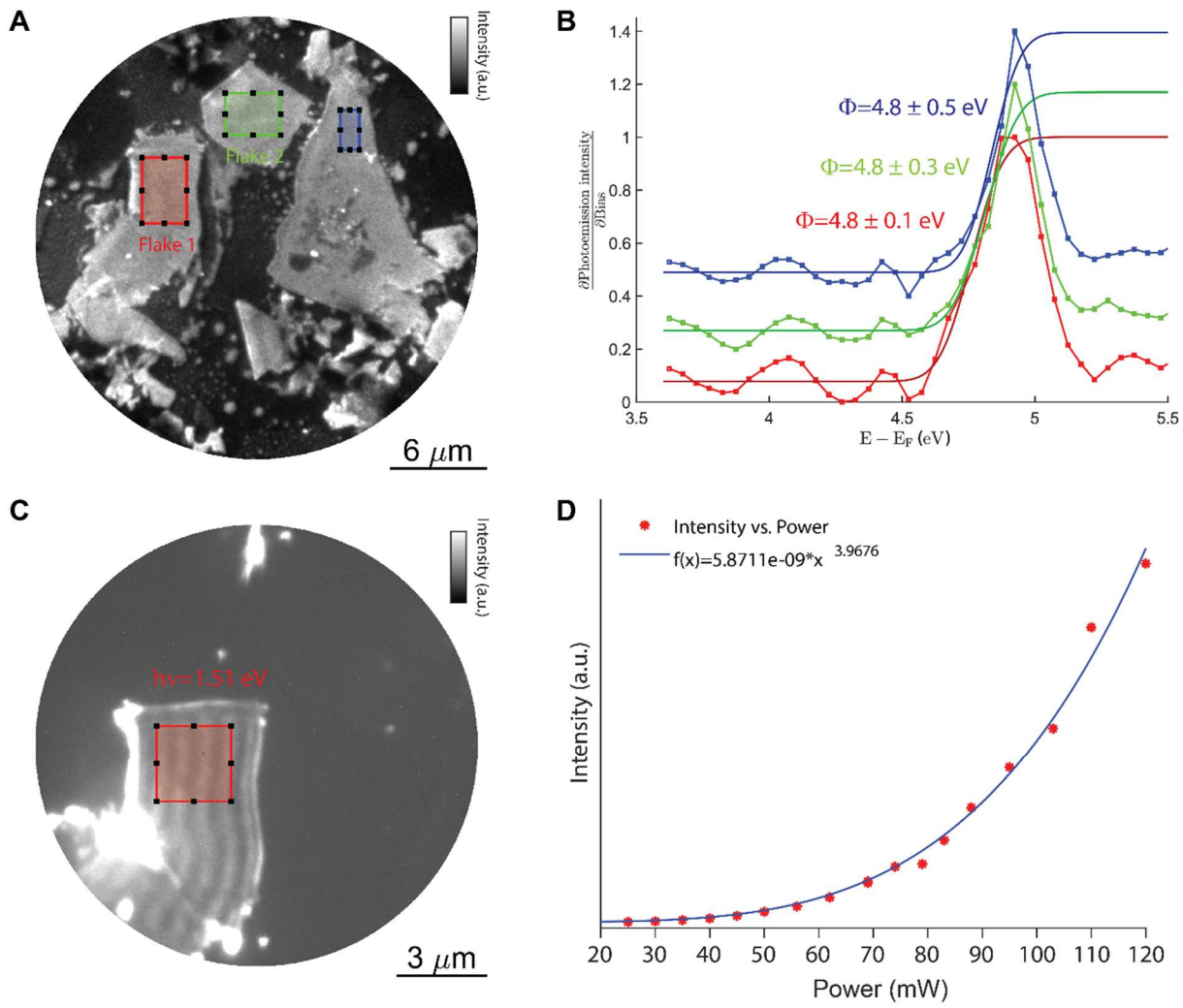

Fig. S6. Surface electronic structure and power-dependence of nP-PEEM on Flake 1 and Flake 2. (A) Energy-integrated 1P-PEEM image of the region where two flakes can be found. (B) Corresponding photoemission spectra from the three regions of interest that are indicated in (A). The work functions, $\boldsymbol{\phi}$, of the three regions of interest were determined by fitting the low energy cutoff of the photoemission spectra with error functions. (C) presents an exemplary nP-PEEM image of the two center flakes at 1.51 eV that was recorded with a laser pulse energy of 18.5 nJ (74mW). (D) shows the spatially integrated photoemission intensity from the region of interest indicated in (C) for varying laser pulse powers. A polynomial function $\boldsymbol{f(x) = A * x^n}$ was fitted to the power-dependent photoemission intensities.

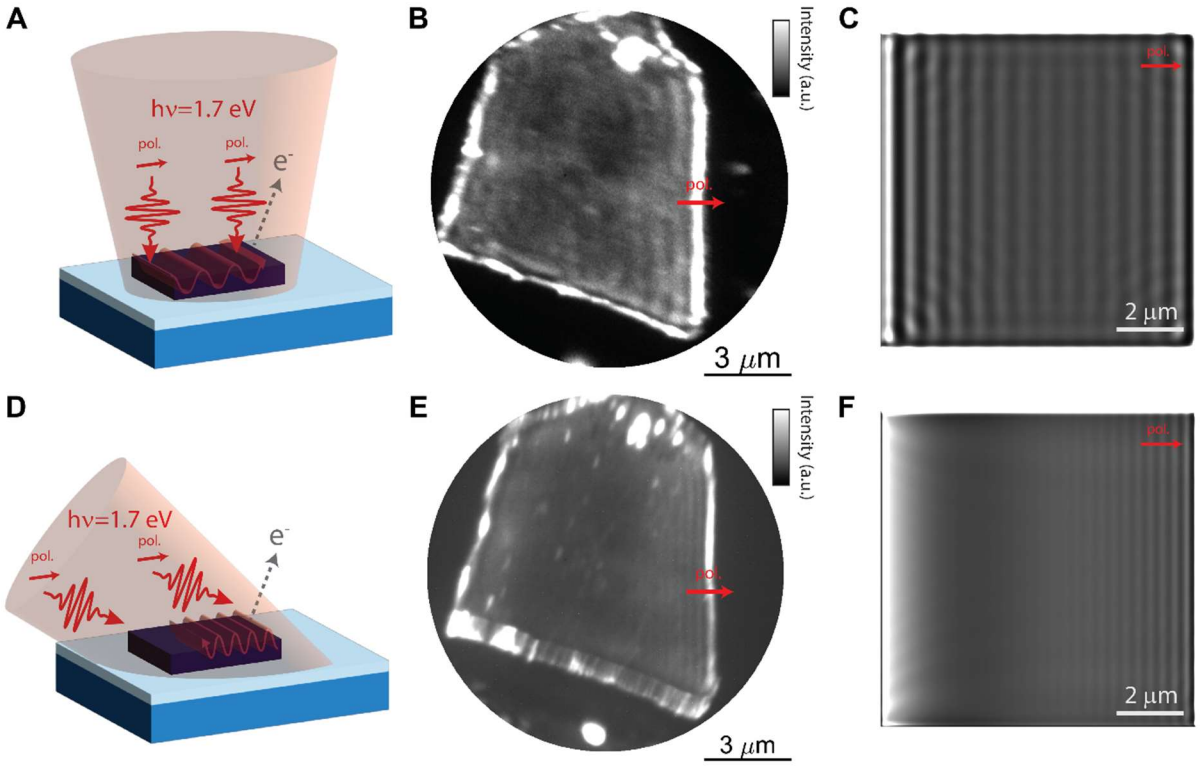

Fig. S7. Comparison of nP-PEEM images from near-normal and grazing laser incidence. (A) Schematic illustration of the launching of fringes on a MXene flake under near-normal incidence. (B) nP-PEEM image of Flake 4 under near-normal incidence at 750 nm (1.7 eV). (C) The simulated near-normal incidence nP-PEEM image of a d=800 nm thick MXene flake on silicon with native oxide at 750 nm. (D) Schematic illustration of fringes on a MXene flake under grazing incidence. (E) nP-PEEM image of Flake 4 under grazing incidence ($\boldsymbol{\theta \approx 4}$°) at 750 nm (1.7 eV). (F) Simulated grazing incidence ($\boldsymbol{\theta \approx 65}$°) nP-PEEM image of a d=800 nm thick MXene flake on silicon with native oxide at 750 nm.

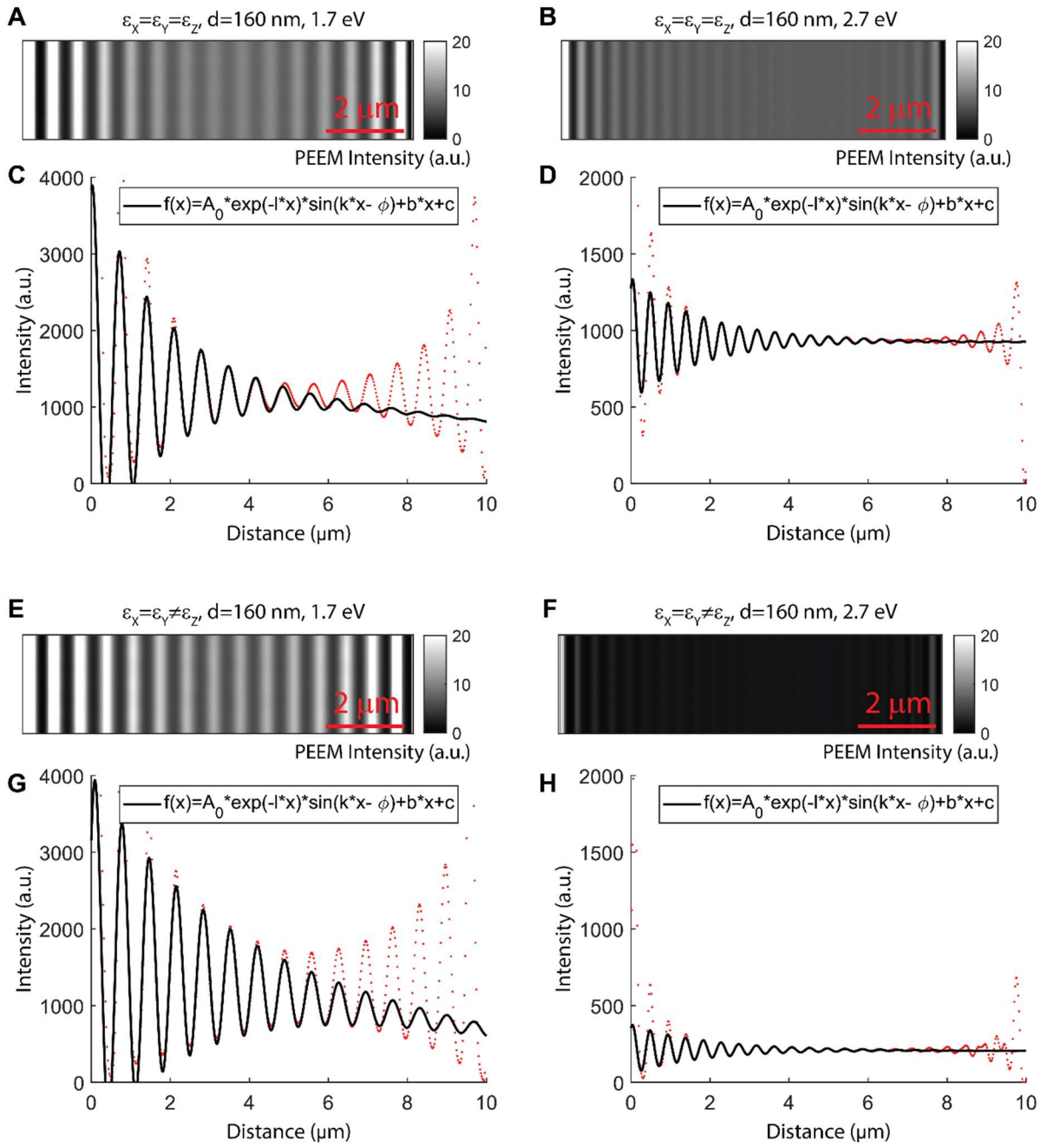

Fig. S8. Impact of an anisotropic dielectric function on nP-PEEM images. (A) FDTD simulated nP-PEEM image at 1.7 eV of a d=160 nm thick isotropic $Ti_3C_2T_x$ flake. (B) FDTD simulated nP-PEEM image at 2.7 eV of a d=160 nm thick isotropic $Ti_3C_2T_x$ flake. (C) and (D) Integrated linecuts from (A) and (B) with corresponding fits. (E) FDTD simulated nP-PEEM image at 1.7 eV of a d=160 nm thick anisotropic $Ti_3C_2T_x$ flake. (F) FDTD simulated nP-PEEM image at 2.7 eV of a d=160 nm thick anisotropic $Ti_3C_2T_x$ flake. (G) and (H) Integrated linecuts from (A) and (B) with corresponding fits.